Chapter 4

Three-Dimensional Lithography Using Combination of Nanoscale Processing and Wet Chemical Etching

Noritaka Kawasegi and Noboru Morita

Additional information is available at the end of the chapter

http://dx.doi.org/10.5772/56354

1. Introduction

Nanofabrication technology is an important field of research, and numerous attempts have been made to improve this technology in recent years. This technology is demanded in various industrial fields such as electronic, photonic, and biomedical engineering to miniaturize machine components. Through miniaturization, the integration and parallelization of components in a machine device are possible, leading to reductions in dead space and fabrication cost. A high-performance device can be fabricated using the changes in physicochemical behavior due to scaling effects; the resonance frequency, thermal response, and chemical reaction all increase with miniaturization. These characteristics are particularly effective in devices such as sensors and reactors. Additionally, Newton's laws of motion do not hold for distances less than 10 nm owing to increased quantum mechanical effects, so that certain types of functions only occur in miniaturized devices. Devices that maximize these effects include microelectromechanical systems and nanoelectromechanical systems, which consist of micro/nanometer-scale mechanical components integrated on a silicon surface.

The conventional fabrication methods of these components are based on photolithography [1], which is a fabrication method used for semiconductor devices. This technique is suitable for mass producing micro/nanostructures because it is a high-throughput fabrication process. It was developed based on Moore's law [2], and it can fabricate sub-100-nm patterns by using deep ultraviolet light with wavelengths of 248 nm and 193 nm. Other major approaches include reactive ion etching [3] and LIGA (lithographie, galvanoformung, abformung) [4], which are mainly used to fabricate high-aspect-ratio structures. However, these fabrication processes use a photomask, which is a high-cost and time-consuming step. Layering and etching techniques are used to fabricate complex structures, but it is difficult to fabricate complex three-dimensional structures. However, several successful attempts have been made to fabricate nano/

micrometer-scale structures using scanning probe microscopy (SPM), focused ion beam (FIB), and electron beam (EB) lithography. Though these methods are effective for fabricating nanometer-scale structures, time-consuming steps are necessary for fabricating sub-micrometer to micrometer-scale structures. Higher and wider structures can be fabricated by taking advantage of the combination of the high resolution of these lithographic techniques and the high-speed material removal of wet chemical etching. Three-dimensional structures can also be fabricated by using this combination of lithography and etching.

Three processing techniques are introduced for three-dimensional fabrication using a combination of nanoscale processing and wet chemical etching. The first is tribo-nanolithography (TNL), which forms an amorphous silicon phase on a silicon substrate by using direct machining, similar to mechanical scratching. The second technique is FIB irradiation, which forms an amorphous phase on a silicon substrate by irradiating it with accelerated ions. The last is EB irradiation, which causes the formation of a thin hydrocarbon layer that has an etch resistance. The etch rate of the processing layer is different from the original material surface, enabling structures to be fabricated after the etching. Additionally, three-dimensional structures can be fabricated using these techniques. The fundamental characteristics and possible applications of these methods are described in the following sections.

2. Three-dimensional fabrication using tribo-nanolithography

2.1. SPM-based lithography

SPM, which includes scanning tunneling microscopy (STM) [5], atomic force microscopy (AFM) [6], and scanning near-field optical microscopy (SNOM) [7], was developed to observe surface characteristics via detecting interactions between a probe and solid materials. The most used instruments in the SPM family are STM and AFM. STM is used to measure the surface topography with atomic resolution by detecting the tunneling current, and AFM measures the topography by detecting minute forces between the probe and the sample. These instruments have a probe and a scanning stage, which means they can be used as a micro tool with a precise stage, similar to a machine tool. Therefore, several micro/nanostructuring technologies arose after the development of these instruments; this technique enabled researchers to manipulate even single atoms [8]. Thus, an SPM can be used as not only a measuring tool but also as a nanostructuring tool, making it appropriate for nanoscale lithography.

SPM lithography can be used to fabricate nanoscale structures by various methods such as electrochemical oxidation [9–11], material transfer [12–14], mechanical removal [15–19] and thermal reaction [21, 22]. This technique is effective for fabricating nanometer-scale structures. However, for fabricating larger structures, time-consuming steps are necessary. The chemical properties of the patterned area change, although the mechanism is different for each method. The patterned area can then be used as an etching mask or it can be selectively etched, and micro/nanometer structures can then be fabricated [9–11, 14, 19]. SPM lithography is used only for the patterning; the structures are fabricated with subsequent etching, which can remove a large amount of material at a time. Thus, SPM lithography with etching is suitable for fabri-

http://dx.doi.org/10.5772/56354

cating structures with a height over several tens of nanometers, whereas SPM lithography alone can only be used for structures that are a few nanometers high. Additionally, three-dimensional structures can be fabricated by controlling the etching mask. Herein we describe a method of three-dimensional fabrication using TNL [19, 22–28] with wet chemical etching.

2.2. Fabrication method

TNL uses AFM as a machine tool for nanopatterning, which enables one to measure the machining forces as well as the machine materials. The technique can be used to machine a material surface with large normal loads by employing a specially designed diamond tip cantilever. The machining setup, based on AFM, is schematically shown in Figure 1(a). The machining forces can be measured from the deflection and torsion of the cantilever, which are both detected by a four-segment photodetector. The normal load is kept constant by a feedback control from a piezo scanner. In the machining process, the specially designed cantilever [18, 29, 30] shown in Figure 1(b) is installed in the system instead of conventional Si_3N_4 or silicon cantilevers. This cantilever has a diamond tip attached to a silicon lever, which has a very high stiffness of more than 1000 times that of conventional cantilevers.

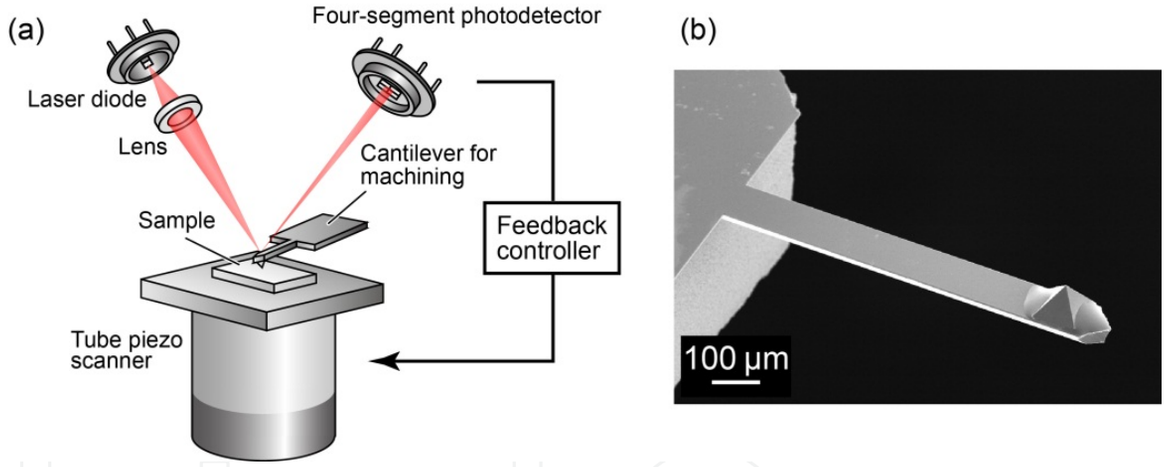

Figure 1. a) Schematic diagram of the experimental setup for TNL based on AFM. (b) SEM image of the cantilever for machining. Reprinted with permission from [29]. Copyright 2006, ASME.

The TNL method forms a modified area on the surface of the silicon substrate via a direct nanomachining method, similar to mechanical scratching. The machining characteristics of the cantilever change significantly owing to the shape of the diamond tip. Figure 2 shows a scanning electron microscopy (SEM) image of cutting tips with different radii. Figure 3 shows AFM topography images of silicon surfaces machined with these cantilevers [30]. When a sharper tip is used, the machined surface is removed and a concave pattern is fabricated, as shown in Figure 3(a) [29, 30]. In this case, continuous cutting chips are formed because the cutting was conducted in a ductile mode owing to the small cutting depth. A dull tip tends not to remove material from the machined area, as shown in Figure 3(b), but instead introduces a high-pressure region to the substrate. Additionally, a 1–2 nm high protuberance was formed,

induced by the volume expansion of the machined area [19, 30]. A dull tip is used in the TNL method because it is more suitable for fabricating precise low-linewidth structures [23].

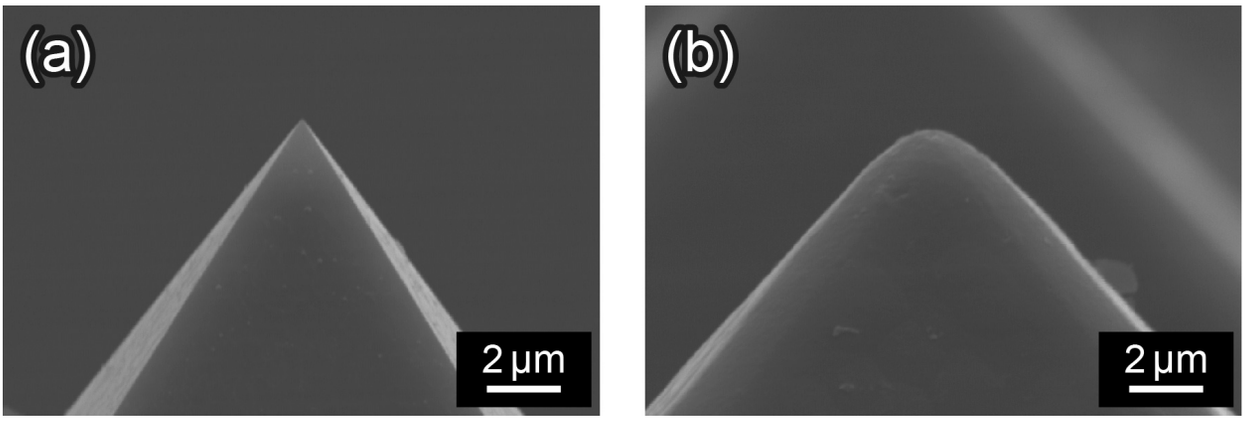

Figure 2. SEM image of diamond tips with (a) sharp and (b) dull cutting edges.

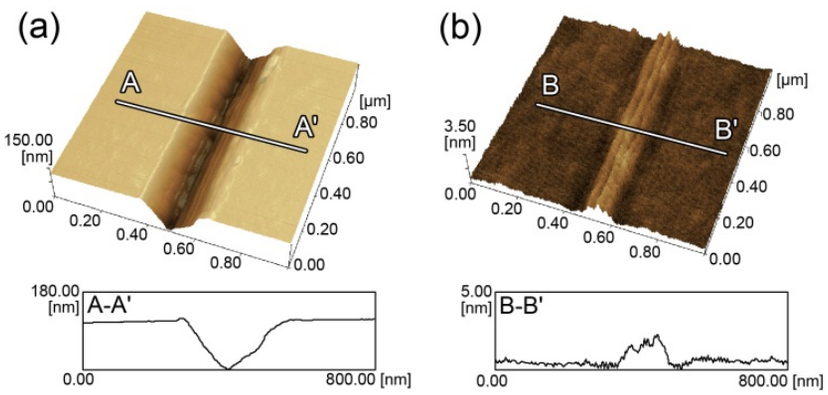

Figure 3. AFM topography images of machined areas. Silicon surfaces were machined with (a) sharp and (b) dull cutting edges at normal loads of 331 µN and 340 µN, respectively.

The fabrication of a structure using a combination of TNL and wet chemical etching is shown in Figure 4 [19]. Figure 4(a) shows an AFM image of the topography of a machined area (15 × 7.5 µm^2 area) prepared using TNL at a normal load of 310 µN and a scanning pitch of 59 nm. The minute protuberance, which is only 1–2 nm high, was formed on the machined area. Figure 4(b) shows an AFM topography image of the same area after etching in a 10 mass% potassium hydroxide (KOH) for 5 min. The machined area was able to resist etching in KOH, whereas the nonmachined area was etched. Thus, a protruding structure with a height of 110 nm was fabricated on the machined area. However, this machined area could also be selectively dissolved in hydrogen fluoride (HF), with the nonmachined silicon surface being barely etched [1]. In this way, a concave structure with a depth of several nanometers to several tens of nanometers could be fabricated from the machined area.

http://dx.doi.org/10.5772/56354

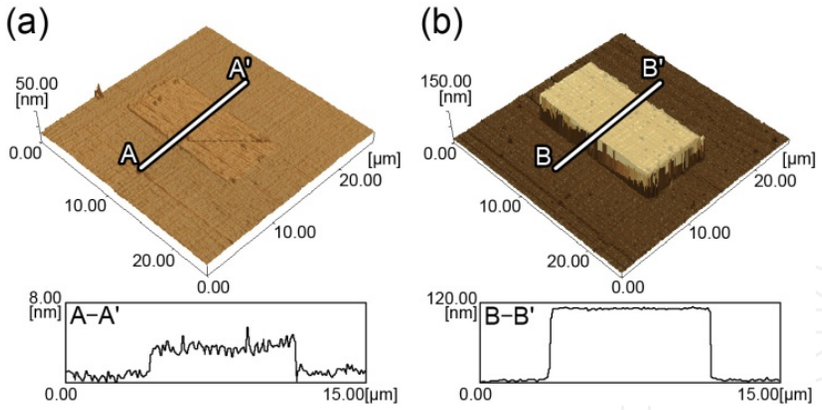

Figure 4. Structure fabrication using a combination of TNL and wet chemical etching. (a) AFM topography image of the machined area (15 × 7.5 μm^2 area) prepared using TNL at a normal load of 310 μN. (b) AFM topography image of the same area after etching in 10 mass% KOH for 5 min. Reprinted with permission from [19]. Copyright 2005, IOP Publishing.

The TNL-induced etch resistance of the machined area is due to the formation of an amorphous phase. Cross-sectional transmission electron microscopy (TEM) images and nano-electron diffraction (nano-ED) patterns of the machined areas prepared by TNL are shown in Figure 5 [19]. Figure 5(a) shows a cross-sectional TEM image of the silicon substrate after machining a single line at a normal load of 350 μN. This image shows that an affected layer measuring 100 nm wide and 15 nm deep was formed. This indicates that the volume expansion of the machined area shown in Figure 4(a) resulted from this layer. The nano-ED pattern of the affected layer in Figure 5(c) shows a diffuse ring pattern, whereas that of the nonmachined area in Figure 5(d) shows a silicon crystal pattern, meaning the machined area was converted to an amorphous phase. Figure 5(b) shows cross-sectional TEM images of the machined area prepared at a scanning pitch of 50 nm. The amorphous phase was thicker than that of a machined single line, and the thickness was observed to be 20 nm. Furthermore, a concave-convex pattern of the silicon crystal structure, which has the same pitch as the scanning pitch, is formed under the amorphous phase. Secondary ion mass spectrometry and Auger electron spectroscopy analyses have shown that the amorphous phase consists entirely of silicon. Therefore, the etch stop effect of the machined area results from the formation of the amorphous phase, rather than from the formation of a chemical compound such as silicon oxide or silicon hydroxide. The TNL-induced amorphous phase was also formed via the removal method, shown in Figure 3(a), by applying the sharp tip with a higher normal load [20]. In this case, a thicker amorphous phase was formed under the machined area as well as large dislocations. The dislocations induced a KOH etching enhancement rather than an etch stop effect. Therefore, in the material removal method, a convex or concave structure can be fabricated by the etching in KOH from the etch stop and etching enhancement effects, which is decided by the concentration of KOH.

The phase transition of the silicon from crystalline to amorphous is due to the high pressure induced by the TNL. During machining, a significantly high pressure is introduced at the contact region of the probe and the silicon substrate, which creates the amorphous silicon phase. Machining-induced phase transitions have been observed during various types of

machining at nano to submicron scales, such as turning [31, 32], grinding [33], indentation [34, 35], and scratching [36, 37]. Silicon, which has a diamond crystal structure, converts to a β-Sn structure at a pressure of approximately 12 GPa, and then converts to an amorphous phase during the pressure release process [37]. This is the mechanism by which the area machined by TNL is converted to an amorphous phase.

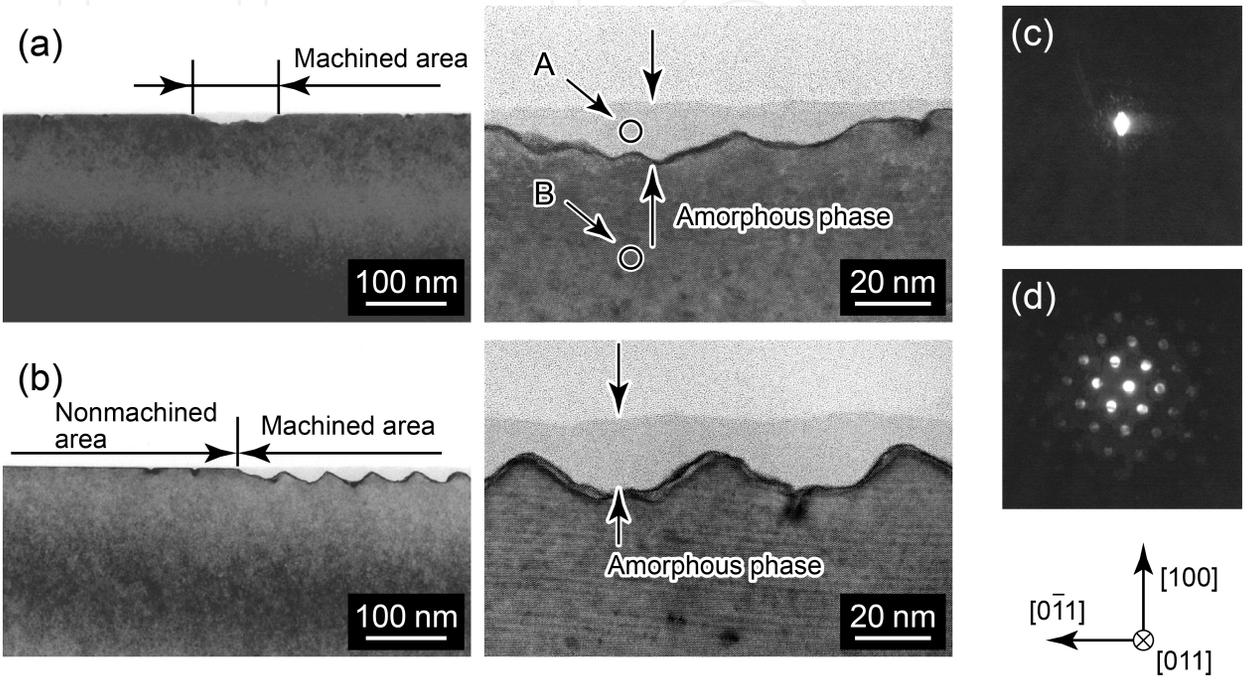

Figure 5. Bright field cross-sectional TEM image of machined area prepared by TNL. (a) Machined area of a single line at a normal load of 350 μN. (b) Machined area prepared at a normal load of 350 μN with a scanning pitch of 50 nm. Nano-ED patterns of a machined area A in (c), and a nonmachined area B in (d). Reprinted with permission from [19]. Copyright 2005, IOP Publishing.

2.3. Three-dimensional fabrication using TNL and wet chemical etching

The morphology of the amorphous phase depends on the machining-induced pressure, and therefore, it can be controlled by the machining conditions. Thus, the change in etch resistance of the amorphous phase can be used to fabricate a three-dimensional structure. The height dependence of the etch rate, the height of the protuberance, and the height of the structure on the normal load is shown in Figure 6 [27]. The silicon surface was machined at various normal loads and then etched in 10 mass% KOH for 10 min. The machined area protruded for normal loads less than 372 μN, whereas the machined area was removed and a concave structure was fabricated for normal loads greater than 372 μN. Therefore, the machining mode is divided into protuberance and removal regions, as shown in the figure. The etch rate of the machined area decreased and the structure height increased with increasing normal loading for the protuberance region. However, the etch rate was nearly constant in the removal region owing to the dislocations formed by the removal machining at higher normal loads. The dislocations enhanced the silicon etching in KOH [22]. Therefore, a constant etch rate at the removal region

http://dx.doi.org/10.5772/56354

resulted from the interaction between the amorphous phase (etch stop effect) and dislocation (etching enhancement effect) formed by the machining. These results demonstrate that the etch resistance can be controlled by the normal load in the protuberance region, whereas it is constant in the removal region. The etch resistance can also be increased by other machining conditions, such as the overlap ratio and number of times the area is machined [23].

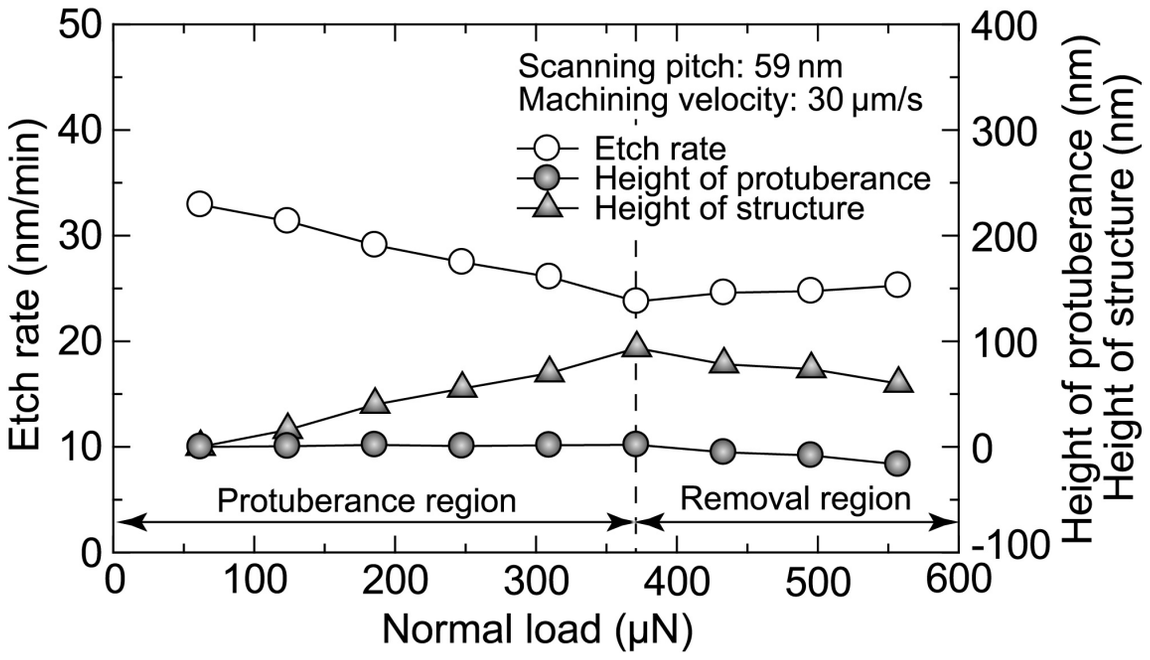

Figure 6. Etch rate of the machined area when the silicon was machined at various normal loads and then etched in 10 mass% KOH for 10 min.

The change in the etch rate of the machined area owing to the machining conditions is caused by the morphology of the amorphous phase. To study this, the morphology of the amorphous phase is measured by etching in HF. Figure 7 shows a cross-sectional TEM image of the machined area prepared at a normal load of 350 μN and a scanning pitch of 50 nm, the same conditions as Figure 5(b), after etching in 25 mass% HF for 10 min [27]. The amorphous phase formed in the machined area was removed, and the concave-convex pattern of the silicon crystal phase remained. The single-crystal silicon surface was scarcely etched in HF [1]. Therefore, the concave structure shown in Figure 7 resulted from the selective removal of the TNL-induced amorphous phase by etching in HF.

Figure 8 shows the thickness of the amorphous phase for various normal loads [27]. The maximum height of protuberance after machining was observed at a normal load of 278 μN. After etching, the depth of the machined area increased with increasing normal load. The amorphous phase was formed by the high-pressure phase transition induced by the TNL [19], and increased in thickness with increasing normal load. Hence, for higher normal loads, a deeper region tended to be transformed to the amorphous phase owing to the high pressure, forming a thicker amorphous phase and resulting in a higher etch resistance against KOH. The

thickness of the amorphous phase is directly correlated to the changes in the etch resistance of the machined area. Alternatively, changes in the etch resistance against KOH due to the scanning pitch and the number of times the area is machined result from the density of the amorphous phase rather than its thickness [27].

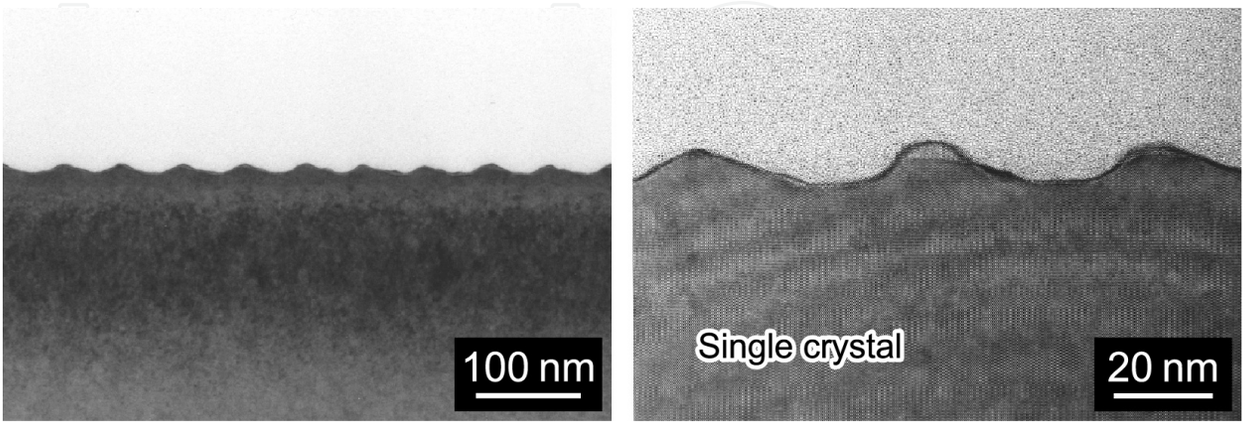

Figure 7. Bright-field cross-sectional TEM image of the machined area after etching in 25 mass% HF for 10 min. The silicon was machined at a normal load of 350 μN and a scanning pitch of 50 nm.

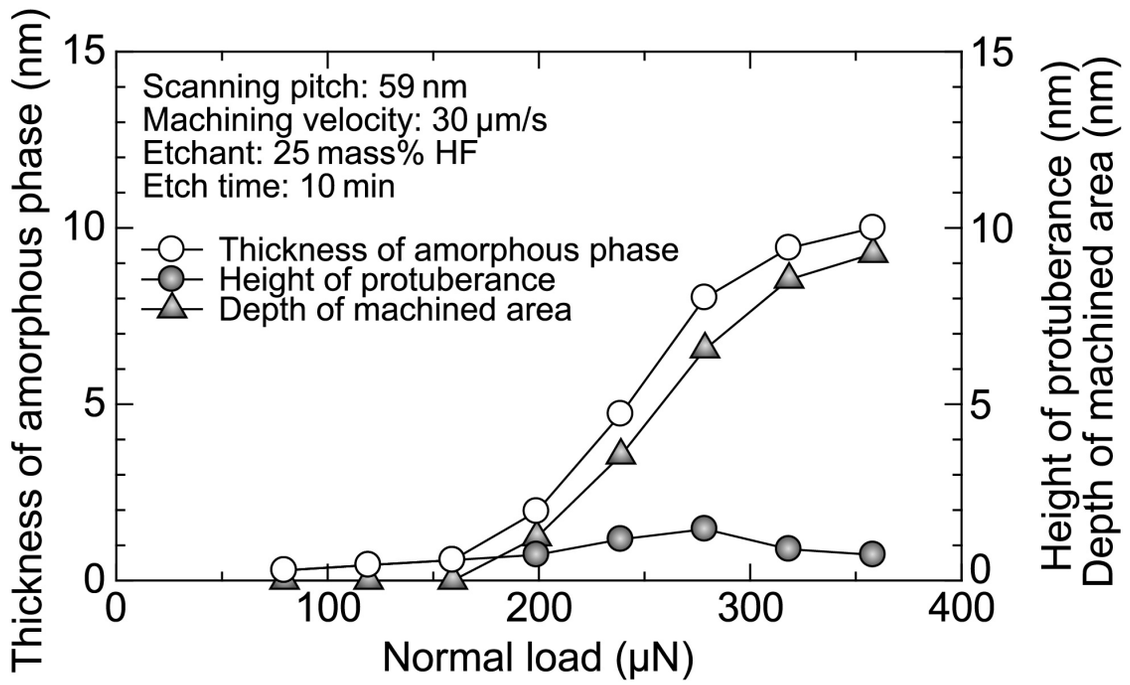

Figure 8. Changes in the thickness of the amorphous phase after the silicon was machined at various normal loads and etched in 25 mass% HF for 10 min.

Figure 9 shows three-dimensional structures with uniform height fabricated by TNL and wet chemical etching. Figures 9(a) shows a "Toyama Prefecture" (located in Japan) pattern.

http://dx.doi.org/10.5772/56354

Structures that are several tens to hundreds of nanometers high can be fabricated using this simple method by machining under constant machining conditions [19]. Figure 9(b) shows a structure with a high aspect ratio fabricated on a (110)-oriented silicon surface. The silicon surface was machined along the <112> direction to take advantage of the anisotropic etching of silicon, and then etched in KOH [28]. This produced structures 150 nm wide and 800 nm high, with an aspect ratio of 5.3. Figure 10 shows a three-dimensional structure fabricated by exploiting the change in the etch resistance with the normal load [23]. The silicon surface was machined using five different normal loads in the range of 124 to 372 μN and protruded to a height of several nanometers after machining, as shown in Figure 10(a). After etching, a stepped structure with five different heights was produced, as shown in Figure 10(b).

This method can be used to fabricate three-dimensional structures with varying heights that cannot be fabricated via conventional photolithographic processes. A three-dimensional sloped structure can also be fabricated by machining while etching in KOH, owing to the simultaneous formation of an amorphous phase with etching [24, 25]. Therefore, this method is effective for various industrial fields in which three-dimensional structures are required.

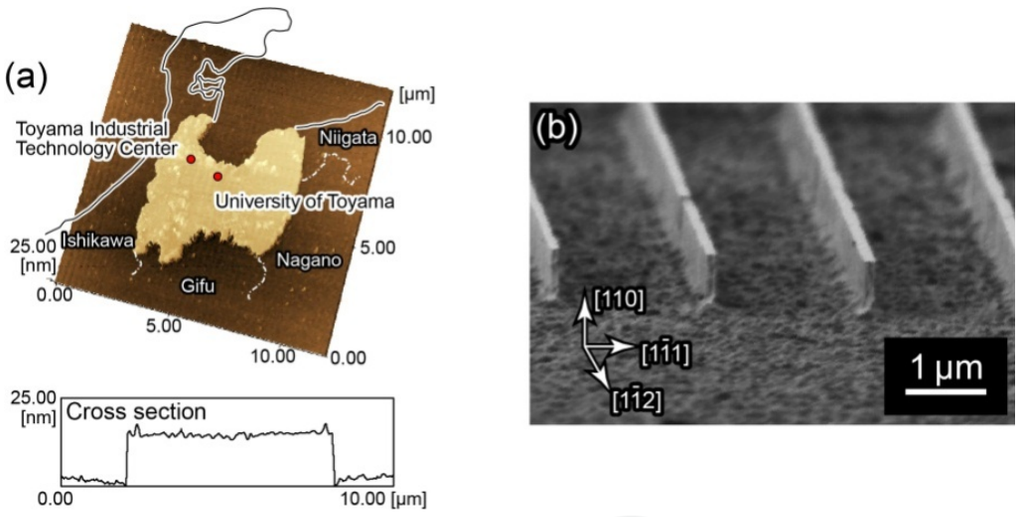

Figure 9. Structures fabricated by TNL and wet chemical etching. (a) AFM topography image of a "Toyama Prefecture" pattern fabricated at a normal load of 350 μN followed by wet chemical etching in KOH for 1 min. (b) SEM image of a high-aspect-ratio structure. The (110)-oriented silicon surface was machined along the <112> direction and then etched in KOH for 12 min.

3. Three-dimensional fabrication using FIB irradiation

3.1. FIB-based lithography

FIB is an instrument that irradiates ions focused over a range of a few nanometers to a few micrometers, accelerating them to an ion energy of 5 to 150 keV [38]. Using FIB, nanostructures can be fabricated by using the interactions of the irradiated ions with substrate atoms and/or introduced gases. The interaction causes sputtering [39–41], deposition [42–44], and implan-

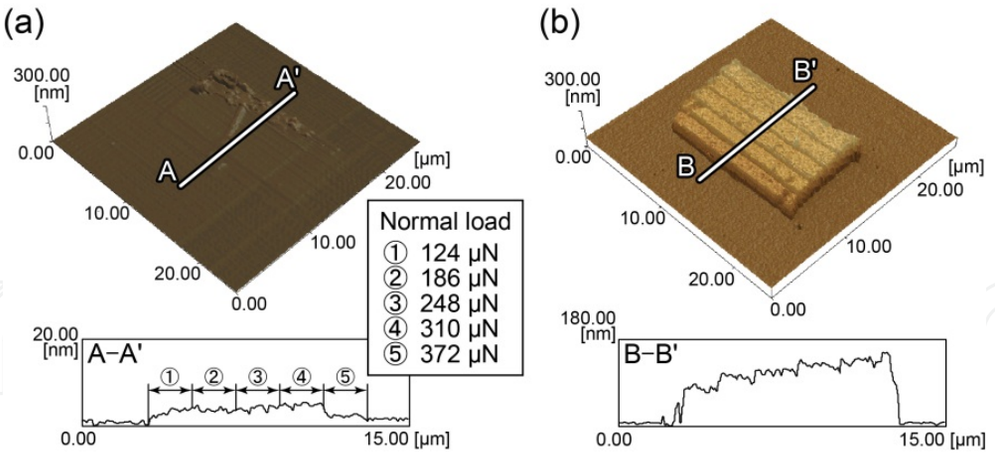

Figure 10. Stepped structure fabricated by TNL and wet chemical etching. (a) AFM topography image of a silicon surface machined using five different normal loads spanning the range of 124 to 372 μN. (b) The same area after etching in 10 mass% KOH for 10 min [27].

tation [45, 46] effects. Sputtering and deposition are used to fabricate nanometer-scale structures, whereas implantation is used to control the electrical properties of the material. FIB methods can be used to machine a sample surface to atomic scales and are thus suitable for fabricating structures that are a few tens of nanometers in size. The most used application of this method is the preparation of TEM samples, for which a thin sample is necessary.

A silicon surface irradiated with ion beams resists some etchants such as KOH [47–55], tetramethylammonium hydroxide [58], sodium hydroxide [50], and hydrazine [56, 57], so that protruding structures can be fabricated via etching. This phenomenon is not dependent on the species of the irradiated ions and has been reported after irradiating Ga [47–53], Si [49, 51, 54–56], Au [49], BF_2 [56], Ni [57], and P [56, 58] ions. The "etch stop" effect of the ion-irradiated area is caused by the formation of an amorphous phase due to ion irradiation [55]. This method is effective for fabricating large structures because the ion irradiation time is significantly shorter than what is required for sputtering and deposition processes. A wet chemical etching process can be used to remove a large amount of material in a short amount of time. The height of the fabricated structure is uniform because the ion-irradiation-induced etching masks have sufficient etch resistance, similar to conventional photolithographic techniques. However, by controlling the etch resistance of the etching mask, the height can be controlled, and therefore, three-dimensional structures can be fabricated. Herein, a three-dimensional fabrication method using FIB irradiation and wet chemical etching [59–61] is described.

3.2. Fabrication method

A fabrication method using a combination of FIB irradiation and wet chemical etching is shown in Figure 11 [59]. Figure 11(a) shows an AFM topography image of a silicon surface area after 30 keV Ga^+ ion irradiation (5 × 5 μm^2 area) at a dose of 13.0 $\mu C/cm^2$. This dose value is significantly lower than that used for structure fabrication via sputtering. This image shows a minute protuberance of the irradiated area, which is only 1–2 nm in height. This phenomenon results

http://dx.doi.org/10.5772/56354

from the formation of an amorphous phase induced by FIB irradiation, similar to the effect of TNL shown in Figure 4(a). Figure 11(b) shows an AFM topography image of the irradiated area after etching in 20 mass% KOH for 5 min. The irradiated area resists etching in KOH, whereas the nonirradiated area is etched, resulting in a protruding structure with a height of 169 nm. The etching characteristics of the irradiated area are different depending on the etchant species. Figure 11(c) shows an AFM topography image of the irradiated area after etching in 46 mass% HF for 20 min. The irradiated area is selectively etched in HF, whereas the nonirradiated area is scarcely etched [1]. Therefore, a concave structure with a depth of 33 nm is fabricated on the irradiated area. This result indicates that the shape of the structure (convex or concave) can be selected by using different etchants.

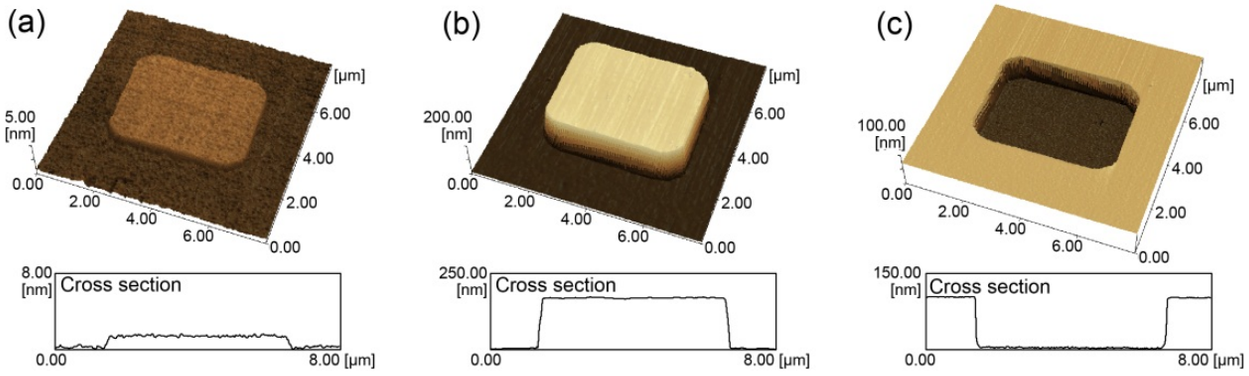

Figure 11. Etching characteristics of a FIB-irradiated area [59, 61]. (a) AFM topography image of a silicon surface after irradiation with 30 keV Ga^+ ions at a dose of 13.0 µC/cm^2. AFM topography image of an irradiated area (b) after etching in 20 mass% KOH for 5 min, and (c) after etching in 46 mass% HF for 60 min.

The difference in the etch resistance against KOH is caused by the thickness and density of the irradiation-induced amorphous phase. Figure 12 shows the cross-sectional TEM images and nano-ED patterns of 30 keV Ga^+ ion-irradiated areas at different doses before and after etching in KOH. An amorphous phase formed in the irradiated area at lower doses, as indicated by the TEM and nano-ED images in Figures 12(a) and (e), respectively. The center of the amorphous phase was 20–30 nm deep, expanding to a depth of 70 nm. The amorphous phase was completely etched, forming a concave–convex pattern on the surface, as shown in Figure 12(b). A thicker and wider amorphous phase formed at a higher dose, as shown in Figure 12(c). The amorphous phase remained after etching, indicating that the amount of silicon etching decreased significantly in the amorphous region. Hence, the etch stop of the irradiated area was caused by the amorphization of silicon. A higher etch resistance resulted from the higher doses owing to the resulting expansion and higher density of the amorphous phase. However, by etching in HF, the amorphous phase was selectively dissolved and a concave structure was fabricated. The depth of the concave structure was determined by the longitudinal expansion of the amorphous phase when HF was used as an etchant.

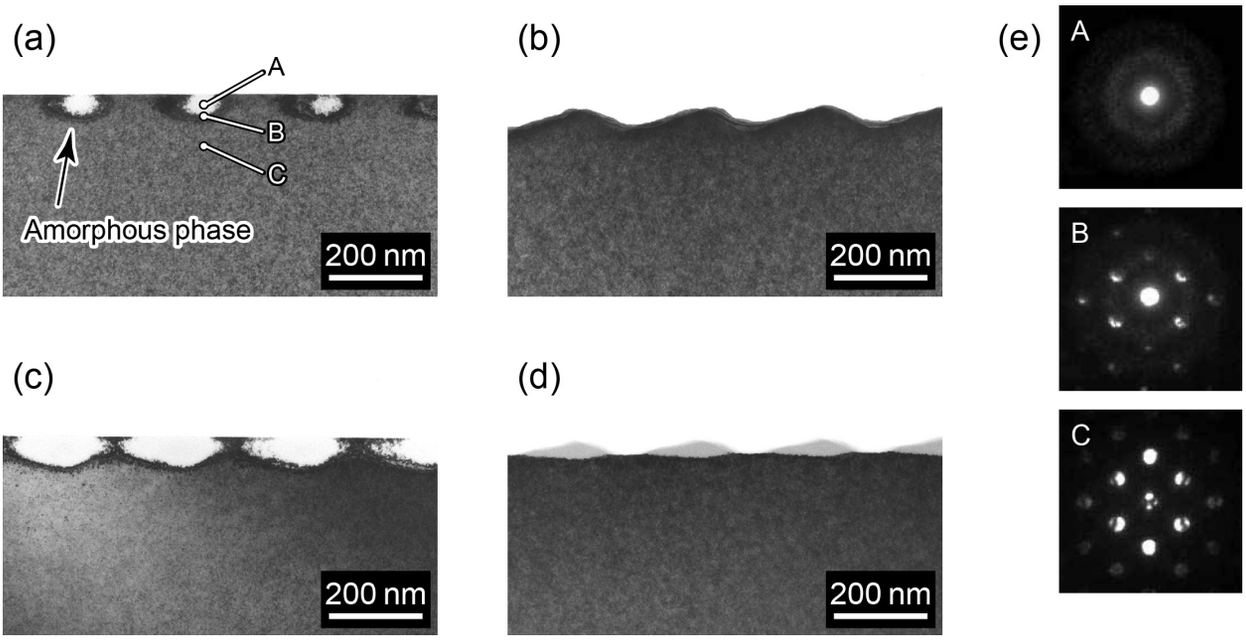

Figure 12. Bright-field cross-sectional TEM images of a 30 keV irradiated area (a) before and (b) after etching in KOH at a low dose, and the irradiated area (c) before and (d) after etching in 20 mass% KOH at a higher dose. Doses per dot in (a) and (c) were 0.9 pC and 1.4 pC, respectively. (e) Nano-ED pattern of the irradiated area denoted by A, B, and C in (a) [59].

As shown in Figure 12, the morphology and the etch rate of the amorphous phase were different according to the irradiation conditions. The height of the structure can be controlled with this technique. Figure 13 demonstrates the relationship between the height of the structure and the ion dose [59]. The silicon surface was irradiated by Ga^+ ions at various doses and then etched in KOH. The etch rate of the irradiated area decreased with increasing ion doses up to 10.0 μC/cm^2. Therefore, higher structures were fabricated using higher doses. For doses over 10.0 μC/cm^2, the etch rate and height were nearly constant at approximately 24 nm/min and 85 nm, respectively. For doses less than 10.0 μC/cm^2, the amorphous phase induced by the ion irradiation was etched, due to the thinner and lower density amorphous phase at low dose condition. The etch resistance at low dose condition varied according to the ion doses, due to the differences in thickness and density of the amourphous phase. Therefore structures of various heights were fabricated owing to the time lag of the dissolution in KOH. A thick and highly dense amorphous phase formed when higher doses of irradiation were used, resulting in a high etch resistance against KOH. The resulting structure was somewhat also etched in KOH because the height of structure was approximately 35 nm lower than the etched depth of the non-irradiated area. This indicates that the amorphous phase formed in the interior of silicon. Therefore, the maximum etch resistance occurred in the interior of silicon, and the resulting height was somewhat less than that of the non-etched area.

The height of the structure can be controlled also by the ion energy. Figure 14 shows the relationship between the ion energy and the height of a structure fabricated after etching in KOH for 5 min [61]. The height of the structure decreased with increasing ion energy at an ion dose of 25 μC/cm^2, whereas the height remained constant at an ion dose of 150 μC/cm^2. For

http://dx.doi.org/10.5772/56354

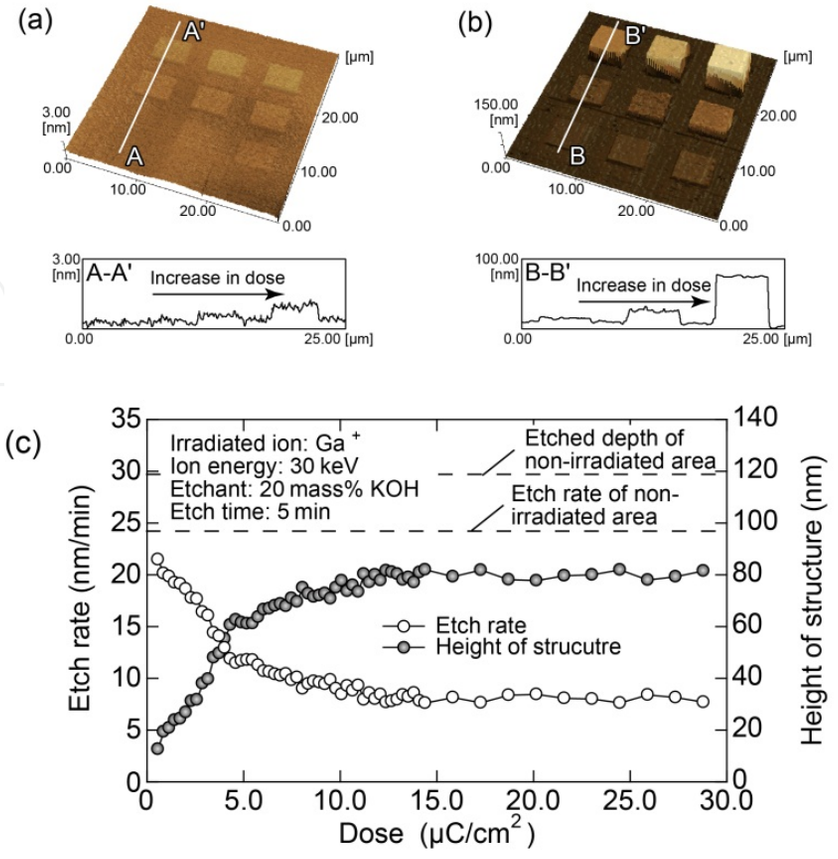

Figure 13. AFM topography image of a FIB-irradiated area at doses of 0.6 to 9.1 μC/cm^2 and an ion energy of 30 keV. (b) The same area after etching in 20 mass% KOH for 5 min. (c) Change in the height of the structure for various ion doses [59].

the lower dose, an amorphous phase formed in the interior of the silicon and the depth of amorphous region increased with the ion energy owing to the dissolution of the non-damaged silicon above the amorphous phase. A lower structure formed at the higher ion energy owing to the increase in the projected range of the irradiated ion. However, an amorphous phase formed from the surface at the higher dose so that the resulting height of the structure was constant for all ion energies. These results indicate that the height of the structure can be controlled by adjusting the ion energy and taking advantage of the difference in depth of the amorphous phase produced by ion irradiation.

A protruding three-dimensional structure can be fabricated by using the methods described above [59]. Figure 15(a) shows an AFM topography image of the stepped structures fabricated using three different doses of FIB irradiation followed by wet chemical etching in KOH. The etch resistance increased with the ion dose, resulting in a higher structure under the high dose condition. Therefore, a single structure with multiple heights can be fabricated by changing the ion dose. Smooth and sloped three-dimensional dome-shaped structures can also be fabricated using this method by continuously changing the ion dose, as shown in Figure 15(b).

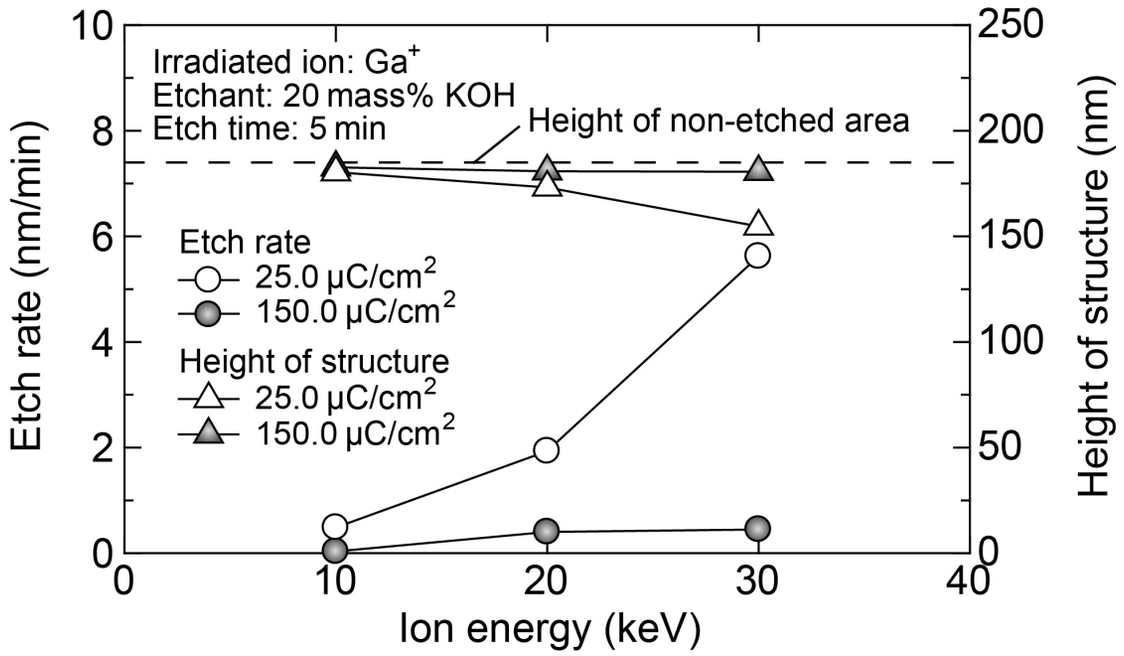

Figure 14. Height change of the structure as a function of the ion energy.

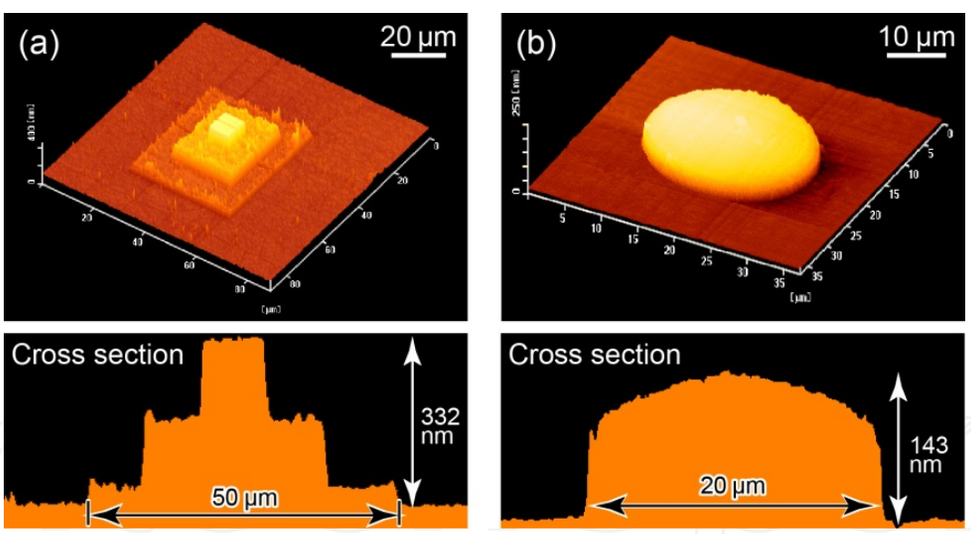

Figure 15. Application of FIB and wet chemical etching to three-dimensional fabrication. AFM topography images of a (a) stepped structure and (b) dome structure [59].

3.3. Three-dimensional fabrication using the etching enhancement

In this section, we describe a three-dimensional fabrication method based on a FIB-induced etching enhancement. In the etching enhancement, the shape of the structure was decided by the morphology of the amorphous phase because the structure was fabricated by the selective dissolution of the amorphous phase. Therefore, a three-dimensional structure was fabricated

http://dx.doi.org/10.5772/56354

using the change in morphology of the amorphous phase according to the ion irradiation conditions.

Figures 16(a) and (c) show AFM topography images of the silicon surface (5 × 5 μm^2 area) irradiated with 30 keV Ga^+ ions at doses of 0.2 to 27.1 μC/cm^2 and 224.0 to 2016.0 μC/cm^2, respectively [61]. The irradiated area protruded at a height of 1 to 2 nm under the lower dose conditions. Under the higher dose conditions, the irradiated area was sputtered and concave structures were fabricated. A burr-like structure also formed around the edge of the irradiated area owing to the reattachment of the sputtered ions. Figures 16(b) and (d) show the AFM topography images of the same areas after etching in 46 mass% HF for 20 min. The irradiated areas were selectively etched in HF, and concave structures were fabricated. In addition, the burr-like structure shown in Figure 16(c) was entirely removed, leaving a smooth surface around the irradiated area. Thus, precise structures could be fabricated in spite of the sputtering that occurs owing to the simultaneous etching of the reattached atoms. However, for lower doses, the irradiated area was scarcely etched.

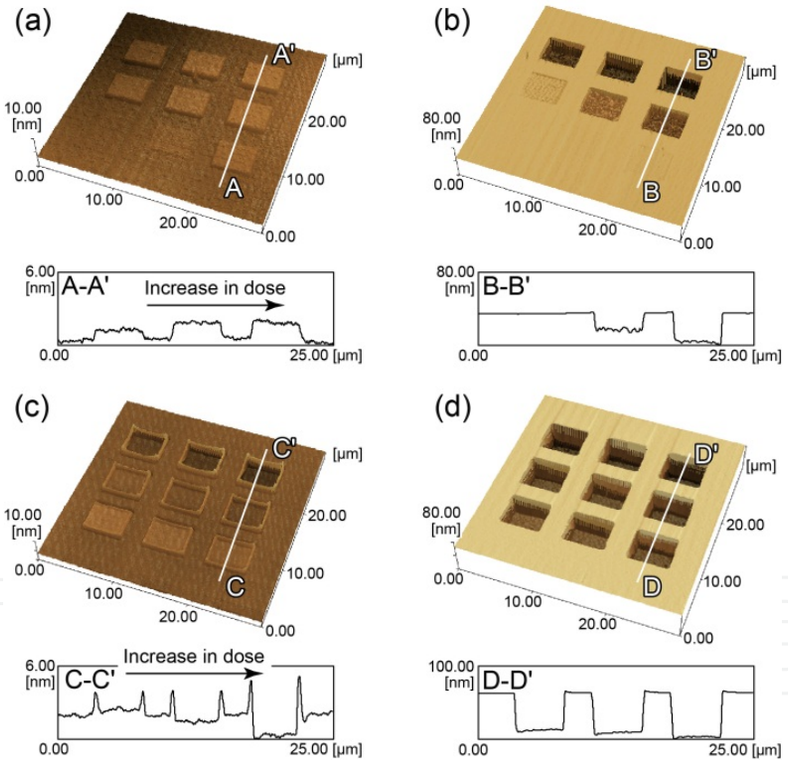

Figure 16. AFM topography image of a silicon surface showing the change in the irradiated area. The areas were irradiated at doses of (a) 0.2 to 27.1 μC/cm^2 and (b) 224.0 to 2016.0 μC/cm^2. (c) and (d) The same areas after etching in 46 mass% HF for 20 min [61].

Figure 17 shows the dependence of the depth of the structure on the dose after etching in HF for 20 min [61]. The irradiated area protruded at a dose of less than 1120 μC/cm^2. At this value, the irradiated area was sputtered and a concave structure was fabricated. The irradiated area was scarcely etched by HF when the dose was less than 6.9 μC/cm^2. The depth of the irradiated

area rapidly increased above this value, whereas a more gradual increase was observed at doses greater than 20.4 μC/cm^2. Amorphization initially occurs near the most heavily damaged region, where most of the irradiated ions have slowed and have low energies, which is shown in Figure 12. Therefore, at lower doses, an amorphous phase is formed in the interior of the silicon near the range of the irradiated ions, while the surface area recrystallizes or is not transformed to an amorphous phase. This crystalline surface layer causes the surface of the irradiated area to be scarcely etched by HF. An amorphous phase forms on the surface at the higher doses owing to the expansion, resulting in dissolution of the irradiated area in HF. A deep structure is fabricated when the dose increases because of the longitudinal expansion of the amorphous phase. Hence, the depth of the structure can be controlled by the ion dose.

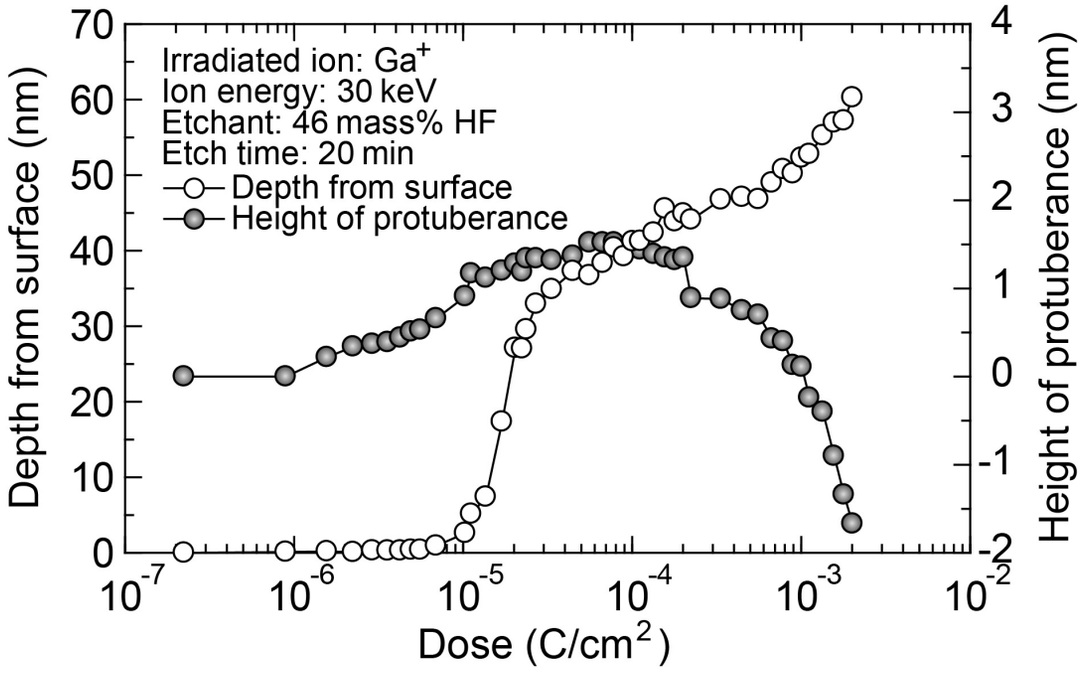

Figure 17. Relationship between the dose and depth from the surface.

The structure depth can also be controlled by the ion energy. Figure 18 shows the relationship between the ion energy and the depth of the structure after etching in HF for 20 min [61]. The depth of the irradiated area was proportional to the ion energy for both doses. The projected range of the irradiated ions increases with the ion energy, resulting in the formation of a thick amorphous phase and therefore a deep structure. Though the maximum depth of the structure was approximately 100 nm owing to the ion energy limitations of conventional FIB instruments, deeper structures over several hundreds of nanometers deep can be fabricated by using a high-energy ion irradiation facility, which can irradiate ions at several hundreds of keV [60].

Because the depth of the structure can be controlled by the ion irradiation conditions such as the dose and the ion energy, a complex three-dimensional structure can be fabricated. Figure 19(a) shows an AFM topography image of a silicon surface irradiated with four different doses

http://dx.doi.org/10.5772/56354

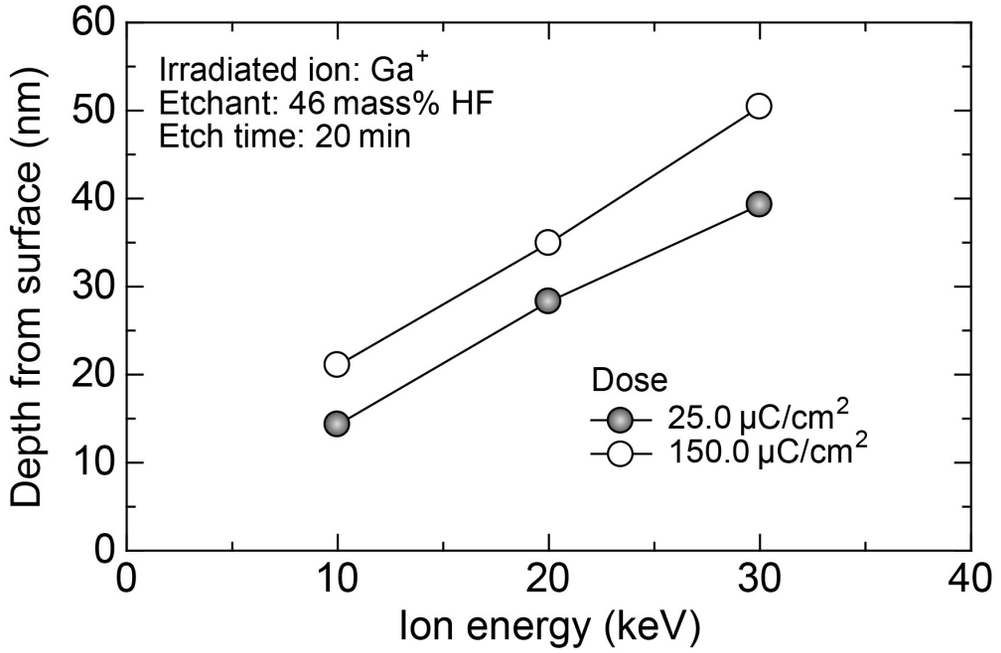

Figure 18. Relationship between the ion energy and depth from the surface.

[61]. The irradiated area protruded owing to the formation of an amorphous phase, but the height difference was only a few nanometers. Figure 19(b) shows an AFM topography image of the same area after etching in 46 mass% HF for 20 min. The depth increased with increasing dose values owing to the change in the thickness of the amorphous phase, and consequently, a stepped structure with four different depths was fabricated from the irradiated area.

Figure 20 shows an AFM topography image of a Fresnel lens pattern structure fabricated by gradually changing the ion dose. This is a three-dimensional structure with a smooth curved surface [61].

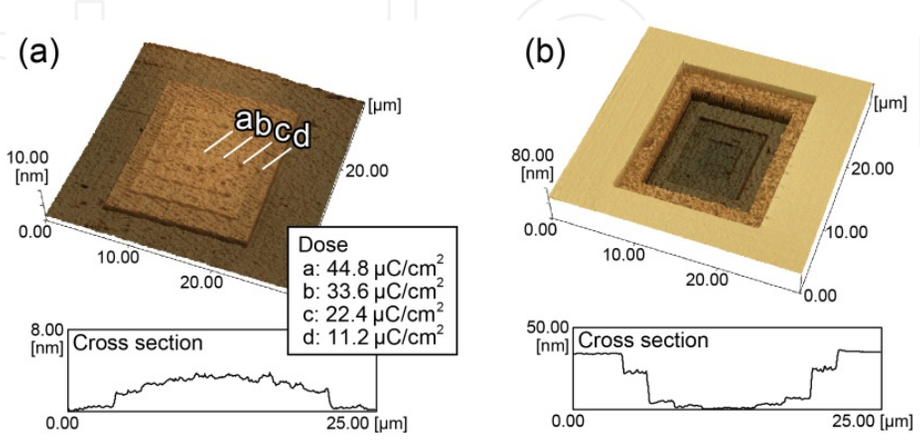

Figure 19. AFM topography image of a three-dimensional structure fabricated by using the change in the etching depth with the ion dose [61].

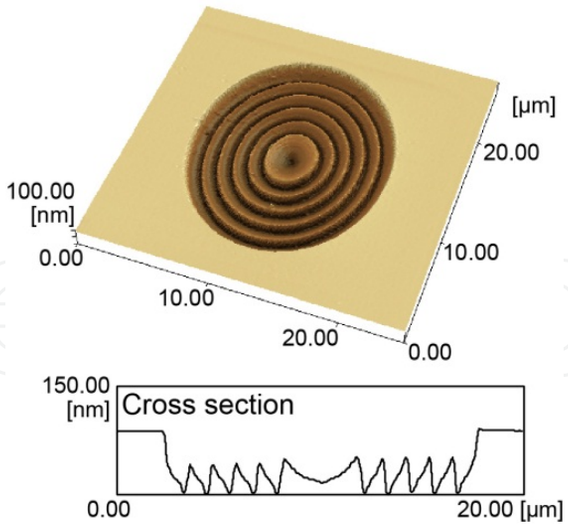

Figure 20. AFM topography image of a Fresnel lens pattern structure fabricated using FIB irradiation with various ion doses followed by wet chemical etching in 46 mass% HF for 20 min [61].

4. Three-dimensional fabrication using electron beam irradiation

4.1. EB-based lithography

The EB is an instrument used for various purposes such as high-resolution surface observation (SEM observation), and resist exposure. In particular, the exposing technique can fabricate fine line patterns in what is known as EB lithography [62], used in a similar way to mask fabrication in photolithography. These methods permit the fabrication of nanometer- or micrometer-scale patterns. However, a more productive method is necessary to fabricate deep and wide structures or complex structures because the direct machining approach requires a time-consuming step. Generally considered contamination, it is known that the EB irradiation causes the formation of a thin hydrocarbon layer on the surface [64–67]. The carbon is introduced by the residual gas and pump into the vacuum chamber. It reacts with the EB and is then deposited on the surface [63]. Because the etching characteristics of the irradiated material change because of EB irradiation, structures can be fabricated efficiently by combining these methods with wet chemical etching, which effectively overcomes the problems of solo-irradiation methods. This method is effective because EB irradiation facilities are used worldwide, and precise patterning, with a minimum line width of several nanometers, is possible using a very simple process. In this session, the three-dimensional fabrication technique using EB-induced carbon deposition [68] is described.

4.2. Fabrication method

Figure 21 shows SEM and AFM images of a GaAs area irradiated using the EB at a dose of 60 mC/cm^2 [68]. The irradiated area appears as a dark area in the SEM image, which indicates the formation of a hydrocarbon layer. This area was raised by 1–2 nm, as shown in Figure 21(b). The hydrocarbon layer has an etch resistance against AH solution, which consists of ammonia

http://dx.doi.org/10.5772/56354

(NH_3), hydrogen peroxide (H_2O_2), and water (H_2O) in a ratio of NH_3:H_2O_2:H_2O = 4:1:3312 by weight. By using this phenomenon, a protruding structure can be fabricated from the irradiated area.

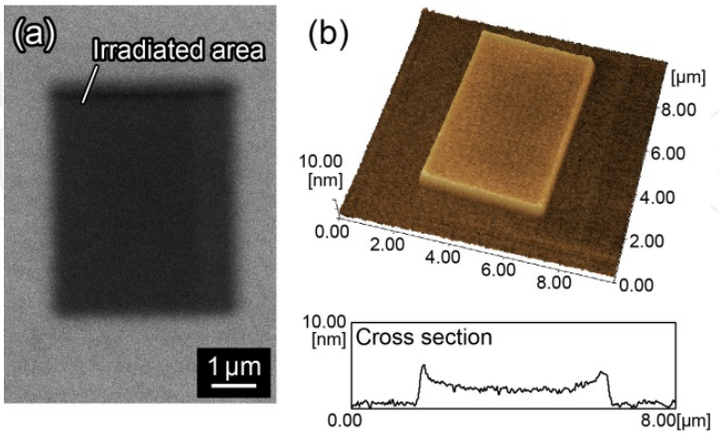

Figure 21. a) SEM and (b) AFM images of the area irradiated at an EB dose of 60 mC/cm^2. Reprinted with permission from [68]. Copyright 2008, IOP Publishing.

4.3. Three-dimensional fabrication using EB irradiation and wet chemical etching

The etch resistance of the irradiated area changes owing to the irradiation conditions, and therefore, the height of the fabricated structure can be controlled via hydrocarbon layers with different etch resistances. By controlling the etch resistance, structures with different heights can be fabricated by taking advantage of the difference in the dissolution time of the hydrocarbon layers. The change in the height of the irradiated area before and after etching in AH solution for 15 s is plotted as a function of the dose in Figure 22 [68]. The height of the hydrocarbon layer ranged from 1–3 nm and increased with the dose. After etching, the irradiated area resisted etching in the AH solution, whereas the nonirradiated area was selectively etched. Consequently, a structure higher than that present before etching was fabricated on the irradiated area. The height of the structure increased with the irradiation dose. With a high dose, a thicker hydrocarbon layer formed on the irradiated area, resulting in a high etch resistance against the AH solution.

Figure 23 shows the change in the height of the structure while etching in AH solution [68]. The increase ratio of the height in the figure denotes the average value between two plots. The height of the structure increased rapidly after etching for 15 s. It remained constant for etch times over 30 s, indicating that the etch-resistant hydrocarbon layer had completely dissolved at 15 s. Additionally, after etching for 15 s, the relative increase in height at 89 mC/cm^2 was greater than the relative increase at 30 mC/cm^2. The values were similar for both dose conditions for etch times over 30 s. Therefore, the difference in the height of a structure according to the irradiation dose results from the difference in the etch rate in the early stages of the etching process. Because the etch resistance of the hydrocarbon layer depends on the concentration of the AH solution, the maximum height of the structure can be controlled by the AH solution concentration [68].

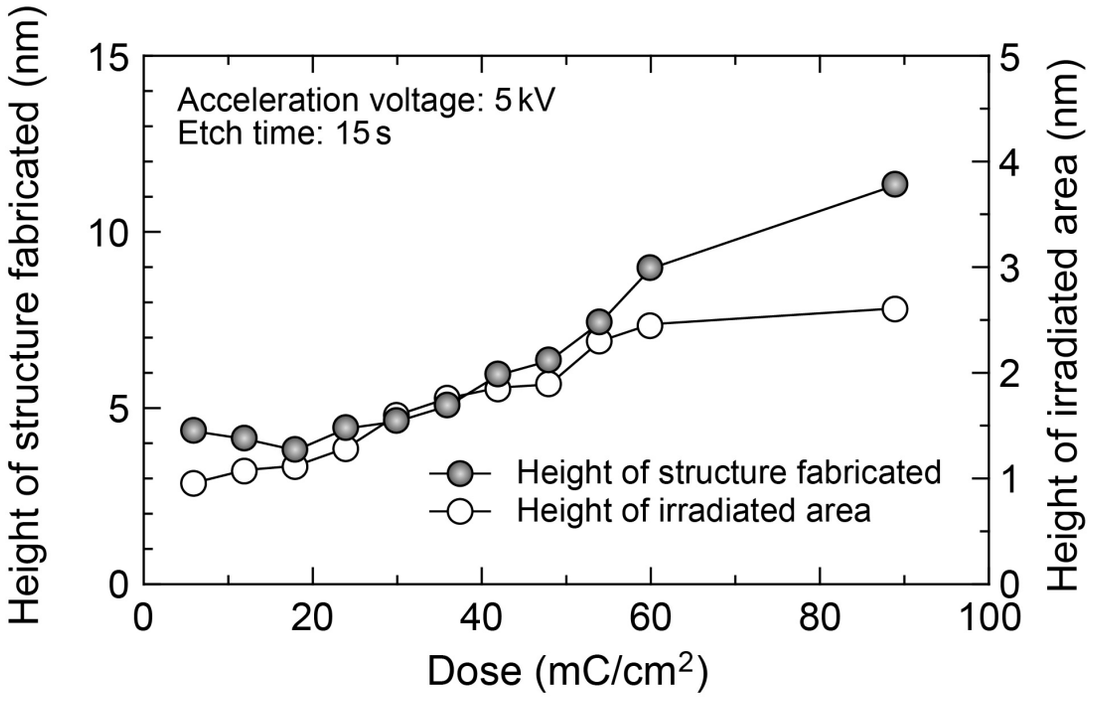

Figure 22. Change in the height of the irradiated area before and after etching in AH solution at various irradiation doses. Reprinted with permission from [68]. Copyright 2008, IOP Publishing.

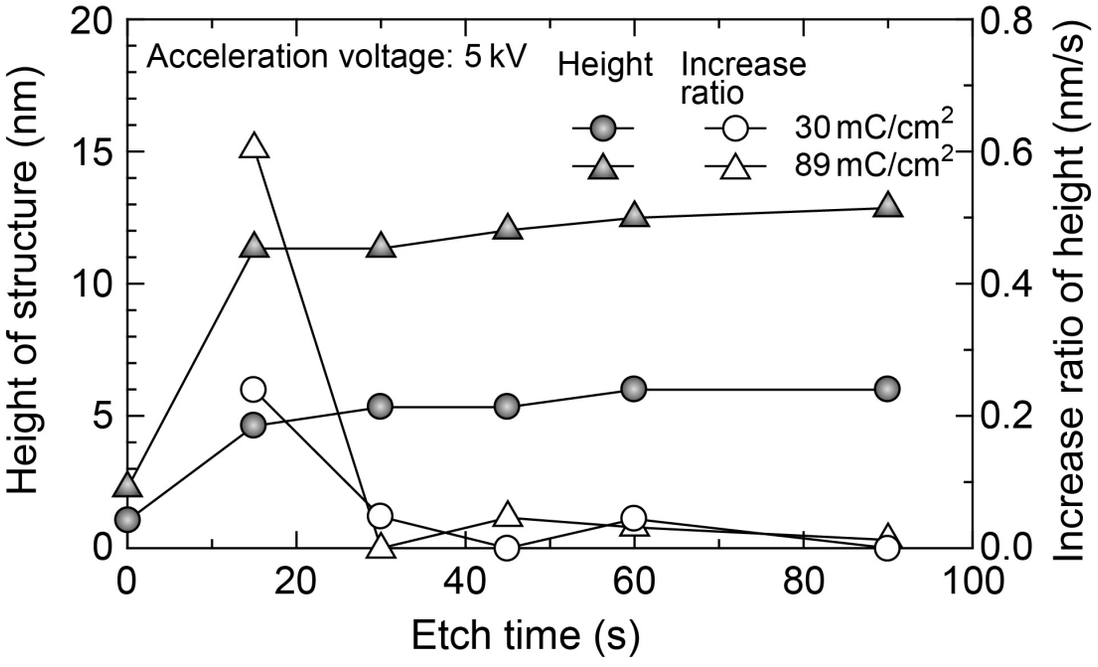

Figure 23. Relationship between the etch time and the height of the structure. The structures were fabricated at different doses. Reprinted with permission from [68]. Copyright 2008, IOP Publishing.

http://dx.doi.org/10.5772/56354

From the results described above, the height of a structure can be controlled by the irradiation condition. Figure 24 shows an AFM topography image of a grating pattern structure with a uniform height, fabricated using constant irradiation conditions [68]. The GaAs surface was irradiated by an EB with a spot size of 1 μm and then etched for 30 s. As a result, structures with a constant height of 12 nm and pitch of 5 μm were fabricated. Figure 24(b) shows an AFM topography image of a three-dimensional structure fabricated by changing the EB dose. The GaAs surface was irradiated with four different doses and then etched for 30 s, resulting in a step structure. The area irradiated with the highest dose is the highest, and the area irradiated with the lowest dose is the lowest.

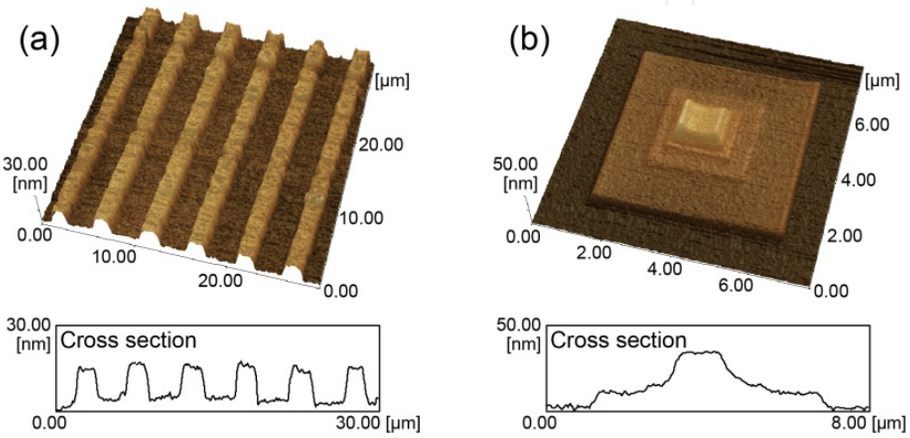

Figure 24. AFM topography images of structures fabricated using EB irradiation and wet chemical etching. (a) A grating pattern structure fabricated using a constant EB dose. (b) A step structure fabricated using the change in etch resistance of the irradiated area with the EB dose. Reprinted with permission from [68]. Copyright 2008, IOP Publishing.

5. Conclusions

We described three-dimensional fabrication techniques using nanoscale processing and wet chemical etching. Three types of processing methods were introduced. We indicated the superiority of these methods for fabricating structures with several tens to hundreds of nanometer high (deep) structures in comparison to conventional photolithographic techniques because they are simpler and more precise. Each of the three processing methods—TNL, FIB, and EB—have distinctive characteristics. Therefore, the processing method should be decided by the desired structure shape, resolution, patterning time, cost, and other factors. TNL simply forms an etching mask because the process is operated in air. The shape is decided by the machining parameters and the tip shape, which is the key technology for this method. FIB forms an etching mask via a rapid process because the dose value needed for the mask fabrication is significantly lower than that needed for a sputtering process. Deeper structures can be fabricated using the FIB-induced etching enhancement. The drawback of this method is the lateral expansion of the irradiated ions and the high-cost instrument. EB forms a high-resolution etching mask using its low-linewidth patterning ability. The maximum height of

the structure was limited to several tens of nanometers and therefore can be improved by patterning and/or etching conditions. The combination of nanoscale processing and wet chemical etching is expected to become an essential tool for emerging nanotechnology and nanoscience applications related to electronic, photonic, biomedical, and nanosystem engineering.

Author details

Noritaka Kawasegi[1*] and Noboru Morita[2]

*Address all correspondence to: kawasegi@itc.pref.toyama.jp

1 Central Research Institute, Toyama Industrial Technology Center, Takaoka, Japan

2 Graduate School of Engineering, Chiba University, Chiba, Japan

References

[1] Elwenspoek, M, & Jansen, H. V. (1998). Silicon Micromachining, Cambridge University Press, Cambridge.

[2] Intel. Moore's Law Inspires Intel Innovation: http://www.intel.com/content/www/us/en/silicon-innovations/moores-law-technology.html (accessed 3 September (2012).)

[3] Kovacs, G. T. A, Maluf, N. I, & Petersen, K. E. Bulk micromachining of silicon. Proc. IEEE (1998). , 86-1536.

[4] Becker, E. W, Ehrfeld, W, Hagmann, P, Maner, A, & Münchmeyer, D. Fabrication of Microstructures with High Aspect Ratio and Great Structural Heights by Synchrotron Radiation Lithography, Galvanoformung and Plastic Moulding (LIGA process). Microelectoron. Eng. (1986). , 4, 35-56.

[5] Binnig, G, & Rohrer, H. Gerber Ch. and Weibel E. Surface Studies by Scanning Tunneling Microscopy. Phys. Rev. Lett. (1982). , 49-57.

[6] Binnig, G, & Quate, C. F. and Gerber Ch. Atomic Force Microscope. Phys. Rev. Lett. (1986). , 56, 930-933.

[7] Pohl, D. W, Denk, W, & Lanz, M. Optical stethoscopy: Image recording with resolution $\lambda/20$ Appl. Phys. Lett. (1984). , 44, 651-53.

[8] Eigler, D. M, & Schweizer, E. K. Positioning single atoms with a scanning tunnelling microscope. Nature (1990). , 344, 524-526.

[9] Dagata, J. A, Schneir, J, Harary, H. H, Evans, C. J, Postek, C. J, & Bennett, J. Modification of hydrogen-passivated silicon by a scanning tunneling microscope operating in air. Appl. Phys. Lett. (1990). , 56, 2001-3.

[10] Chien, F. S. S, Wu, C. L, Chou, Y. C, Chen, T. T, Gwo, S, & Hsieh, W. F. Nanomachining of (110)-oriented silicon by scanning probe lithography and anisotropic wet etching. Appl. Phys. Lett. (1999). , 75-2429.

[11] Snow, E. S, Campbell, P. M, & Shanabrook, B. V. Fabrication of GaAs nanostructures with a scanning tunneling microscope. Appl. Phys. Lett. (1993). , 63, 3488-90.

[12] Kolb, D. M, Ullmann, R, & Will, T. Nanofabrication of Small Copper Clusters on Gold(111) Electrodes by a Scanning Tunneling Microscope. Science (1997). , 275, 1097-99.

[13] Piner, R. D, Zhu, J, Xu, F, Hong, S, & Mirkin, C. A. Dip-Pen" Nanolithography. Science (1999). , 283, 661-3.

[14] Weinberger, D. A, Hong, S, Mirkin, C. A, Wessels, B. W, & Higgins, T. B. Combinatorial generation and analysis of nanometer- and micrometer-scale silicon features via "dip-pen" nanolithography and wet chemical etching. Adv. Mater. (2000). , 12, 1600-3.

[15] Mccord, M. A, & Pease, R. F. Scanning tunneling microscope as a micromechanical tool. Appl. Phys. Lett. (1987). , 50, 569-71.

[16] Magno, R, & Bennett, B. R. Nanostructure patterns written in III-V semiconductors by an atomic force microscope. Appl. Phys. Lett. (1997). , 70, 1855-7.

[17] Lee, H. T, Oh, J. S, Park, S. J, Park, K. H, Ha, J. S, Yoo, H. J, & Koo, J. Y. Nanometer-scale lithography on H-passivated Si(100) by atomic force microscope in air. J. Vac. Sci. Technol. A (1997). , 15, 1451-4.

[18] Ashida, K, Morita, N, & Yoshida, Y. Study on nano-machining process using mechanism of a friction force microscope. JSME Int. J. Ser. C (2001). , 44, 244-53.

[19] Kawasegi, N, Morita, N, Yamada, S, Takano, N, Oyama, T, & Ashida, K. Etch stop of silicon surface induced by tribo-nanolithography. Nanotechnology (2005). , 16, 1411-4.

[20] Ashida, K, Chen, L, & Morita, N. New maskless miro-fabrication technique of single crystal silicon using the combination of nanometer-scale machining and wet etching. Balsamo A., Evans C., Frank A., Knapp W., Mana G., Mortarino M., Sartori S. Thwaite E.G. (Eds.) Proceedings of 2nd european society for precision engineering and nanotechnology, May 27th-31st, 2001, Turin, Italy; (2001).

[21] Vettiger, P, Despont, M, Drechsler, U, Durig, U, Haberle, W, Lutwyche, M. I, Rothuizen, H. E, Stutz, R, Widmer, R, & Binnig, G. K. The 'millipede'-more than one thousand tips for future AFM data storage. IBM J. Res. Develop. (2000). , 44, 323-40.

[22] Bae, J. H, Ono, T, & Esashi, E. Scanning probe with an integrated diamond heater element for nanolithography. Appl. Phys. Lett. (2003). , 82, 814-6.

[23] Kawasegi, N, Morita, N, Yamada, S, Takano, N, Oyama, T, Ashida, K, & Micro-fabrication, D. using Combination Technique of Nano-scale Processing and Chemical Etching (1st Report, Possibility of 3D micro-fabrication using the mechanism of friction force microscope). Trans. Jpn. Soc. Mech. Eng. C (in Japanese) (2004).

[24] Kawasegi, N, Park, J. W, Morita, N, Yamada, S, Takano, N, Oyama, T, & Ashida, K. Nanoscale fabrication in aqueous KOH solution using tribo-nanolithography. J. Vac. Sci. Technol. B (2005). , 23, 2471-5.

[25] Park, J. W, Kawasegi, N, Morita, N, & Lee, D. W. Tribonanolithography of silicon in aqueous solution based on atomic force microscopy. Appl. Phys. Lett. (2004). , 85, 1766-8.

[26] Park, J. W, Kawasegi, N, Morita, N, & Lee, D. W. Mechanical approach to nanomachining of silicon using oxide characteristics based on tribo nanolithography (TNL) in KOH solution. ASME J. Manuf. Sci. Eng. (2004). , 126, 801-6.

[27] Kawasegi, N, Morita, N, Yamada, S, Takano, N, Oyama, T, & Ashida, K. Morphological control of a tribo-nanolithography-induced amorphous silicon phase for three-dimensional lithography. J. Adv. Mecha. Des. Sys. Manuf. (2007). , 1, 283-93.

[28] Kawasegi, N, & Morita, N. High-aspect ratio structure fabrication on (110)-oriented silicon surfaces using tribo-nanolithography. J. Nanosci. Nanotechnol. (2010). , 10, 2394-400.

[29] Kawasegi, N, Takano, N, Oka, D, Morita, N, Yamada, S, Kanda, K, Takano, S, Obata, T, & Ashida, K. Nanomachining of silicon surface using atomic force microscope with diamond tip. ASME J. of Manuf. Sci. Eng. (2006). , 128, 723-9.

[30] Kawasegi, N, Fukase, T, Takano, N, Morita, N, Yamada, S, Kanda, K, Takano, S, Obata, T, & Ashida, K. Development and its applications of diamond array tool using silicon mold (2nd report)-Fabrication of machining cantilever with arbitrary tip shape-J. Jpn. Soc. Prec. Eng. (2006). in Japanese).

[31] Shibata, T, Ono, A, Kurihara, K, Makino, E, & Ikeda, M. Cross-section transmission electron microscope observations of diamond-turned single-crystal Si surfaces. Appl. Phys. Lett. (1994). , 65, 2553-5.

[32] Yan, J. Laser micro-Raman spectroscopy of single-point diamond machined silicon substrates. J. Appl. Phys. (2004). , 95, 2094-101.

[33] Puttick, K. E, Whitmore, L. C, Chao, C. L, & Gee, A. E. Transmission electron microscopy of nanomachined silicon crystals. Phil. Mag. (1994). , 69, 91-103.

[34] Clarke, D. R, Kroll, M. C, Kirchner, P. D, Cook, R. F, & Hockey, B. Amorphization and conductivity of silicon and germanium induced by indentation. J. Phys. Rev. Lett. (1998). , 60, 2156-9.

[35] Bradby, J. E, Williams, J. S, Wong-leung, J, Swain, M. V, & Munroe, P. Transmission electron microscopy observation of deformation microstructure under spherical indentation in silicon. Appl. Phys. Lett. (2000). , 77, 3749-51.

[36] Gogotsi, Y, Baek, C, & Kirscht, F. Raman microspectroscopy study of processing-induced phase transformations and residual stress in silicon. Semicond. Sci. Tech. (1999). , 14, 936-44.

[37] Gogotsi, Y, Zhou, G, Ku, S, & Cetinkunt, S. S. Raman microspectroscopy analysis of pressure-induced metallization in scratching of silicon. Semicond. Sci. Technol. (2001). , 16, 345-52.

[38] Orloff, J, Utlaut, M, & Swanson, L. High resolution focused ion beam: FIB and Its Application. New York: Kluwer Academic / Plemium Pulication; (2003).

[39] Efremow, N. N, Geis, M. W, Flanders, D. C, Lincoln, G. A, & Economou, N. P. Ion-beam-assisted etching of diamond. J. Vac. Sci. Technol. B (1985). , 3, 416-8.

[40] Hopkins, L. C, Griffith, J. E, Harriott, L. R, & Vasile, M. J. Polycrystalline tungsten and iridium probe tip preparation with a Ga+ focused ion beam. J. Vac. Sci. Technol. B (1995). , 13, 335-7.

[41] Russell, P. E, Stark, T. J, Griffis, D. P, Phillips, J. R, & Jarausch, K. F. Chemically and geometrically enhanced focused ion beam micromachining. J. Vac. Sci. Technol. B (1988). , 16, 2494-8.

[42] Gamo, K, Takakura, N, Samoto, N, Shimizu, R, & Namba, S. Ion beam assisted deposition of metal organic films using focused ion Beams. Jpn. J. Appl. Phys. (1984). L, 293-5.

[43] Matsui, S, Kaito, K, Fujita, J, Komuro, M, Kanda, K, & Haruyama, Y. Three-dimensional nanostructure fabrication by focused-ion-beam chemical vapor deposition. J. Vac. Sci. Technol. B (2000). , 18, 3181-4.

[44] Fujita, J, Ishida, M, Ichihashi, T, Ochiai, Y, Kaito, T, & Matsui, S. Growth of three-dimensional nano-structures using FIB-CVD and its mechanical properties. Nucl. Instr. and Meth. B (2003). , 206, 472-7.

[45] Reuss, R. H, Morgan, D, Greeneich, E. W, Clark, W. M, & Rensch, D. B. Vertical npn transistors by maskless boron implantation. J. Vac. Sci. Technol. B (1985). , 3, 62-6.

[46] Evason, A. F, Cleaver, J. R. A, & Ahmed, H. Focused ion implantation of gallium arsenide metal-semiconductor field effect transistors with laterally graded doping profiles. J. Vac. Sci. Technol. B (1988). , 6, 1832-5.

[47] Berry, I. L, & Caviglia, A. L. High resolution patterning of silicon by selective gallium doping. J. Vac. Sci. Technol. B (1983). , 1, 1059-61.

[48] La Mache PH., Levi-Setti R. and Wang Y.L. Focused ion beam microlithography using an etch-stop process in gallium-doped silicon. J. Vac. Sci. Technol. B (1983). , 1, 1056-8.

[49] Steckl, A. J, Mogul, H. C, & Mogren, S. Localized fabrication of Si nanostructures by focused ion beam implantation. Appl. Phys. Lett. (1992). , 60, 1833-5.

[50] Schmidt, B, Bischoff, L, & Teichert, J. Writing FIB implantation and subsequent anisotropic wet chemical etching for fabrication of 3D structures in silicon. Sensors Actuators A (1997). , 61, 369-73.

[51] Fuhrmann, H, Döbeli, M, & Mühle, R. Focused ion-beam structuring of Si and Si/$CoSi_2$ heterostructures using adsorbed hydrogen as a resist. J. Vac. Sci. Technol. B (1999). , 17, 945-8.

[52] Edenfeld, K. M, Jarausch, K. F, Stark, T. J, Griffis, D. P, & Russell, P. E. Force probe characterization using silicon three-dimensional structures formed by focused ion beam lithography. J. Vac. Sci. Technol. B (1994). , 12, 3571-5.

[53] Kawasegi, N, Morita, N, Yamada, S, Takano, N, Oyama, T, Ashida, K, Taniguchi, J, Miyamoto, I, & Momota, S. Etching characteristics of a silicon surface induced by focused ion beam irradiation. Int. J. Manuf. Technol. Manag. (2006).

[54] Fuhrmann, H, Döbeli, M, Kötz, R, Mühle, R, & Schnyder, B. Thin oxides on passivated silicon irradiated by focused ion beams. J. Vac. Sci. Technol. B (1999). , 17, 3068-71.

[55] Fuhrmann, H, Candel, A, Döbeli, M, & Mühle, R. Minimizing damage during focused-ion-beam induced desorption of hydrogen. J. Vac. Sci. Technol. B (1999). , 17, 2443-6.

[56] Koh, M, Sawara, S, Goto, T, Ando, Y, Shinada, T, & Ohdomari, I. New process for si nanopyramid array (NPA) fabrication by ion-beam irradiation and wet etching. Jpn. J. Appl. Phys. (2000). , 39, 2186-8.

[57] Koh, M, Goto, T, Sugita, A, Tanii, T, Iida, T, Shinada, T, Matsukawa, T, & Ohdomari, I. Novel Process for high-density buried nanopyramid array fabrication by means of dopant ion implantation and wet etching. Jpn. J. Appl. Phys. (2001). , 40, 2837-9.

[58] Masahara, M, Matsukawa, T, Ishii, K, Liu, Y, Nagao, M, Tanoue, H, Tanii, T, Ohdomari, I, Kanemaru, S, & Suzuki, E. Fabrication of ultrathin Si channel wall for vertical double-gate metal-oxide-semiconductor field-effect transistor (DG MOSFET) by using ion-bombardment-retarded etching (IBRE). Jpn. J. Appl. Phys. (2003). , 42, 1916-8.

[59] Kawasegi, N, Morita, N, Yamada, S, Takano, N, Oyama, T, Ashida, K, & Micro-fabrication, D. using combination technique of nano-scale processing and chemical etch-

ing (2nd report, possibility of 3D micro-fabrication using focused ion beam process). Trans. Jpn. Soc. Mech. Eng. C (2004). in Japanese).

[60] Kawasegi, N, Morita, N, Yamada, S, Takano, N, Oyama, T, Momota, S, Taniguchi, J, & Miyamoto, I. Depth control of a silicon structure fabricated by 100q keV ar ion beam lithography. Appl. Surf. Sci. (2007). , 253-3284.

[61] Kawasegi, N, Morita, N, Yamada, S, Takano, N, Oyama, T, Ashida, K, Taniguchi, J, & Miyamoto, I. Three-dimensional nanofabrication utilizing selective etching of silicon induced by focused ion beam irradiation. JSME Int. J. Ser. C (2006). , 49, 583-9.

[62] Yamazaki, K, Yamaguchi, T, & Namatsu, H. Three-Dimensional Nanofabrication with nm Resolution. Jpn. J. Appl. Phys. (2004). L1111-3., 10.

[63] Djenizian, T, Santinacci, L, & Schmuki, P. Factors in electrochemical nanostructure fabrication using electron-beam induced carbon masking. J. Electrochem. Soc. (2004). G, 175-80.

[64] Miura, N, Ishii, H, Shirakashi, J, & Yamada, A. and Konagai M Electron-beam-induced deposition of carbonaceous microstructures using scanning electron microscopy. Appl. Surf. Sci. (1997). , 114-269.

[65] Djenizian, T, Salhi, B, Boukherroub, R, & Schmuki, P. Bulk micromachining of silicon using electron-beam-induced carbonaceous nanomasking. Nanotechnology (2006). , 17-5363.

[66] Djenizian, T, Santinacci, L, Hildebrand, H, & Schmuki, P. Electron beam induced carbon deposition used as a negative resist for selective porous silicon formation. Surf. Sci. (2003). , 524-40.

[67] Chen, I. C, Chen, L. H, Orme, C, Quist, A, Lal, R, & Jin, S. Fabrication of high-aspect-ratio carbon nanocone probes by electron beam induced deposition patterning. Nanotechnology (2006). , 17-4322.

[68] Morita, N, Kawasegi, N, & Ooi, K. Three-dimensional fabrications on gaas surfaces using electron beam-induced carbon deposition followed by wet chemical etching Nanotechnology (2008).

IntechOpen